Three-dimensional hard X-ray micro-tomographic imaging of the human palatal anatomy and gracilis muscle

Daphne Schönegg*[a,b], Hans Deyhle[a], Georg Schulz[a,c], Christine Tanner[a], Sharif Ahmed[d], Robert Atwood[d], Andreas A. Mueller[e,f], Magdalena Müller-Gerbl[g], Szilvia Mezey[g], Richard L. Lieber[h], Ali Khounsary[i], and Bert Müller[a]

[a]Biomaterials Science Center, Department of Biomedical Engineering and Department of Clinical Research, University of Basel, Hegenheimermattweg 167b, 4123 Allschwil, Switzerland

[b]Department of Cranio-Maxillofacial Surgery, Inselspital, Bern University Hospital, Freiburgstrasse 20, 3010 Bern, Switzerland

[c]Core Facility Micro- and Nanotomography, Department of Biomedical Engineering, University of Basel, Hegenheimermattweg 167c, 4123 Allschwil, Switzerland

[d]Diamond Light Source, Fermi Ave, Didcot, Oxfordshire, OX11 0DE, United Kingdom

[e]Department of Oral and Craniomaxillofacial Surgery, University Hospital Basel and University Children's Hospital Basel, 4031 Basel, Switzerland

[f]Facial and Cranial Anomalies Research Group, Department of Biomedical Engineering and Department of Clinical Research, University of Basel, Spitalstrasse 21, 4031 Basel, Switzerland

[g]Institute of Anatomy, Department of Biomedicine, University of Basel, Pestalozzistrasse 20, 4056 Basel, Switzerland

[h]Shirley Ryan Ability Lab, Northwestern University, 355 East Erie Street, 60611 Chicago, Illinois, United States of America

[i]Department of Physics, Illinois Institute of Technology, 10 West 35th Street, 60616 Chicago, Illinois, United States of America

ABSTRACT

Palatoplasty in infants with cleft palate aims to reconstruct the intricate three-dimensional anatomy and restore the velopharyngeal function, which is essential for swallowing, speech, and ventilation of the middle ear through the opening of the Eustachian tube. The non-destructive analysis of the microarchitecture around the pterygoid hamulus using hard X-rays should enhance the existing knowledge from dissection and histological studies. Specifically, the micro-anatomical relationship between the palatine aponeurosis, the tendon of the tensor veli palatini muscle, and the pterygoid hamulus must be characterized to understand their structural relationship and functional implications. At the cellular level, the arrangement of fibers within muscle fascicles needs to be clarified. The right half of a historical plastinated infant cadaveric head was examined with two laboratory-based micro computed tomography (μCT) systems: phoenix|xray nanotom® m for imaging of the entire specimen with a pixel size of 55 μm; and Zeiss Xradia 610 Versa for local tomography with a pixel size of 3.4 μm. Using synchrotron radiation-based microtomography, additional measurements were performed with a pixel size of 3.24 μm. The resulting images were rigidly registered and analyzed. Automated threshold-based segmentation of bones and manual segmentation of muscles, tendons, and aponeurosis, were performed to visualize their topographic relationships in three dimensions. An unstained segment of a human gracilis muscle was examined using the Exciscope Polaris with a pixel size of 0.35 μm, and the fiber architecture was visually inspected. Laboratory-based X-ray μCT systems are suitable for virtual-histology examination of soft tissues and visualization of subcellular structures therein. Synchrotron radiation-based μCT with phase retrieval provided additional contrast within the plastinated soft tissues. The findings of this study support the hypothesis that the palatal muscles form a complex muscle sling around the pterygoid hamulus, underscoring the importance of preserving this bony protuberance during cleft palate repair.

Keywords: Micro computed tomography, phase-contrast tomography, image registration, segmentation of anatomical features, cleft palate, palatoplasty, pterygoid hamulus anatomy, human gracilis muscle.

*daphne.schoenegg@insel.ch; phone +41 31 632 33 17; https://www.bmc.unibas.ch

Developments in X-Ray Tomography XV, edited by Bert Müller, Ge Wang,
Proc. of SPIE Vol. 13152, 1315229 · © 2024 SPIE
0277-786X · doi: 10.1117/12.3035601

1. INTRODUCTION

Surgical approaches to cleft palate repair have advanced significantly since they were first described over 200 years ago, yet consensus on the optimal technique remains elusive, and practices continue to vary among surgeons [1]. Reconstruction of the velopharyngeal muscular sphincter and lengthening of the soft palate are critical to develop a physiologic swallowing pattern, ensure proper ventilation of the middle ear via the Eustachian tube, and prevent hyper-nasal speech [2]. Techniques such as tensor tenotomy or fracturing of the pterygoid hamulus can help achieve tension-free palatal closure, thereby preventing velopharyngeal insufficiency and potentially minimizing the impact on facial growth [1]. However, these maneuvers may also compromise muscle function and impede the physiologic opening of the Eustachian tube during swallowing by altering the biomechanical behavior of the pharyngeal muscle sling [3].

The pterygoid hamulus, a hook-like projection of the medial pterygoid plate of the sphenoid bone, acts as a fulcrum for the velopharyngeal muscle sling, as determined in anatomical studies using dissection, staining and histology [4, 5]. Variability in specimen preparation, dissection techniques and specimen characteristics has affected the interpretation of the local micro-anatomy in such dissection studies, and there are few imaging studies on this topic, leaving some uncertainty regarding the anatomy. Key muscles in the region include the tensor veli palatini muscle and the superior pharyngeal constrictor muscle.

The tensor veli palatini muscle is commonly described as a single muscle with two origins, one at the cranial base and one at the Eustachian tube, converging at a common insertion point in the palatine aponeurosis, a firm layer of connective tissue that forms the basis for attachment of the soft palate muscles [6, 7]. However, more comprehensive investigations indicate that this may be an oversimplification of the anatomy, as the muscle appears to consist of two independent parts with separate origins and insertion points. The lateral head of the tensor veli palatini muscle runs from the cranial base, laterally to the Eustachian tube, anteriorly and downward to the pterygoid hamulus, which diverts it anteromedially to its mobile insertion at the palatine aponeurosis. The medial head originates from the cartilaginous and membranous part of the Eustachian tube and connects to the base of the pterygoid hamulus, which serves as a fixed insertion point. This medial head has also been referred to as part of the *musculus dilatator tubae* complex [8], although this term is commonly used to describe the function of several muscles involved in the opening of the Eustachian tube and thus not included in the *terminologia anatomica* [9].

Cleft surgery needs to mobilize the aponeurosis to unify it in the midline. Normal auditory tube function should be preserved. Therefore, a better understanding of the tensor-aponeurotic-palatal anatomy should help to improve surgical approaches to the cleft palate.

The minute scale of the pterygoid hamulus and the palatal muscles in newborns presents a challenge to conventional visualization methods. Clinical imaging techniques suitable for high-resolution visualization, such as specialized MRI, are technically and procedurally demanding in infants, and ethical considerations limit access to post-mortem infant or fetal specimens. Cleft surgery is usually performed in infancy, and given the considerable anatomical differences between fetuses or adults and infants, the study of infant anatomy is most useful for surgical conclusions [10]. Historical specimens from anatomical museums serve as an invaluable alternative resource, offering a vast selection that allows researchers to select the most appropriate specimen for their specific needs. The well-preserved specimens can be examined with high-resolution laboratory-based imaging modalities, which are infeasible for clinical use. This approach not only addresses specific medical or technical research questions in an ethical manner but also contributes to the documentation of unique museum specimens.

Hard X-ray micro computed tomography (μCT) has recently been applied for virtual histology, *i.e.*, for the non-destructive visualization of tissues at resolutions comparable to light microscopy [11, 12]. The high-resolution isotropic imaging enables detailed three-dimensional segmentation and rendering of anatomical structures, thereby advancing the understanding of complex topographical relationships. Studies on iodine-stained fetal specimens have demonstrated the applicability of μCT in visualizing palatal anatomy with remarkable clarity [13-15]. Advanced μCT has also been used for the investigation of the microstructure of skeletal muscle tissue, further underscoring its suitability for muscle imaging [16, 17]. Less discussed aspects of muscle micro-anatomy include the micro-topography of the muscle-bone interface,

which has been studied mostly with scanning electron microscopy in dry human tissue [18], and the microscopic arrangement of muscle fibers within long skeletal muscles [19].

This study employs laboratory- and synchrotron-based X-ray μCT systems to examine a historical specimen of an infant cadaveric head, aiming to enhance the understanding of palatal muscle attachments and configuration around the pterygoid hamulus. The synchrotron radiation-based data of the same specimen should provide additional insights and allow for a comprehensive comparison of imaging modalities including benchmarking. Laboratory-based μCT of formalin-preserved human skeletal muscle tissue seeks to visualize the fiber arrangement at the cellular level. In addition to demonstrating the applicability of laboratory-based μCT for high-resolution visualization of the palatal anatomy and unstained muscle tissue, this study aimed to analyze the pterygoid hamulus and its muscular surroundings and to demonstrate the micro-architecture of a large human skeletal muscle. The results of this preliminary study might also contribute to a better understanding of the surgical anatomy in palatoplasty and help define the most appropriate approach to cleft palate repair.

2. MATERIALS AND METHODS

2.1 Specimens

A historical specimen obtained from the Institute of Anatomy at the University of Basel, Switzerland, was examined. The specimen, the right half of an infant's head (estimated time of death in the neonatal period) with no known craniofacial abnormalities, was preserved by plastination. Due to the absence of accompanying documentation, details of the plastination process or the history of the specimen remain unknown. Prior to this study, a conventional computed tomography (CT) scan, as used in the clinics (Siemens SOMATOM Emotion 16-slice scanner with a tube voltage of 130 kV), was performed on the specimen, which confirmed that the relevant anatomical structures around the pterygoid hamulus were intact and well preserved, thus making the specimen suitable for more detailed examination using advanced imaging techniques. The photograph in Figure 1 shows the region of interest.

Figure 1. Sagittal view of the historical plastinated cadaveric infant head specimen showing the well-preserved hard (◆) and soft (✱) palate, size of the area shown: 38 mm × 22 mm. Photo courtesy of the Anatomical Museum, University of Basel, Switzerland.

An excess segment of a human gracilis muscle donated to researchers at Northwestern University's Feinberg School of Medicine, Chicago, United States of America, after medically indicated surgery, was used for a preliminary μCT study. The specimen was placed in 10 % buffered formalin solution for a duration of 48 hours immediately after harvest, rinsed three times in phosphate-buffered saline (PBS), and then transferred to PBS for storage. After an initial laboratory-based μCT scan in PBS, the muscle sample was dehydrated in an ascending ethanol series in 10 % increments for a period of one hour each, starting with 50 % ethanol and 50 % distilled water. It was then stored in 100 % ethanol at room temperature for the study. Figure 2 shows photographs of the muscle part before and after ethanol dehydration to illustrate the changes in shape and related shrinkage.

According to current Swiss legislation, research involving anonymized biological material does not require prior authorization from an ethics committee. Therefore, no ethics approval had to be obtained for this study.

Figure 2. Segment of a human gracilis muscle after storage in phosphate-buffered saline (top) and after dehydration in an ascending ethanol series to 100 % ethanol (bottom). One can clearly recognize the preparation-induced tissue shrinkage, which amounts to approximately 15 %. The distance between adjacent background markings is 7.5 mm.

2.2 Laboratory-based microtomography studies

The plastinated head specimen was examined with two laboratory-based µCT systems, with the acquisition parameters listed in Table 1. Projections were acquired over 360° in all three setups.

Table 1. Acquisition parameters for the laboratory-based micro computed tomography study of the cadaveric infant head.

Parameter	**GE nanotom® m**	**Zeiss Xradia 610 Versa**	
		(a)	**(b)**
Source-detector distance [mm]	310.0	232.5	231.5
Source-object distance [mm]	170.5	118.0	118.0
Geometrical magnification	1.82	1.97	1.96
Optical magnification	1	0.4	4
Acceleration voltage [kV]	170	100	110
Beam current [µA]	30	140	141
Filter	0.5 mm Cu	LE6 (equivalent to 1.3 mm Al)	
Effective pixel size [µm]	55	34.8	3.4
Number of projections	1800	2401	6001
Exposure time per projection [s]	18	5	25

A full-field scan was obtained using the nanotom® m system (phoenix|x-ray, GE Sensing & Inspection Technologies GmbH, Wunstorf, Germany) equipped with a 3072 × 2400 pixel flat-panel detector. The specimen was placed horizontally in a 5 cm thick polystyrene block in which a recess corresponding to the specimen's outer shape had been manually cut.

The polystyrene block was secured to the sample stage with a putty-type adhesive (Blu Tack®, Bostik SA, Colombes, France).

The Zeiss Xradia 610 Versa system (Carl Zeiss X-ray Microscopy, Inc., Dublin, California, USA) was used to acquire two local tomography datasets of the region of interest around the pterygoid hamulus. This system uses a 2048 × 2048 pixel CCD sensor and variable optical magnification through selected objectives. The first scan was registered with the 0.4× objective and is referred to as (a). The second scan with the 4.0× objective was centered on the pterygoid hamulus using the integrated automatic focusing function: "Scout-and-Scan Control System" and referred to as (b). For both scans, the specimen was placed in a 3D-printed cylindrical holder that had been designed based on the segmentation of the conventional CT scan of the specimen, as shown in Figure 3. This holder positioned the specimen at an inclination of approximately 4° counterclockwise relative to the Frankfurt horizontal plane. This axis had been defined from the nanotom® m scan to ensure passage of the X-ray beam between the highly X-ray absorbing structures, *i.e.* the cochlea and the calcified tooth buds, into the area of interest for a more uniform X-ray absorption. The specimen holder was fixed on the sample stage with a typecleaner (Typutz, Läufer, Burgdorf, Germany) in an eccentric position so that the center of rotation was aligned with the hamular region.

Figure 3. 3D-printed specimen holder that had been designed using a conventional computed tomography scan of the specimen with the matching 3D-printed replica of the specimen placed inside the holder.

The human gracilis muscle fascicle was examined in a standard thin-walled plastic pipette tip sealed with wax at the bottom and Parafilm M (Amcor, Victoria, Australia) at the top that was filled with PBS or ethanol using the Exciscope Polaris (Exciscope AB, Kista, Stockholm, Sweden). The system is equipped with a liquid metal X-ray source, a 2048 × 2048 pixel detector and three objectives. The high-resolution scan in ethanol employing the 20× objective was focused on a region where the fiber architecture appeared diverse in the overview scan and was extended over 360°. The acquisition parameters are detailed in Table 2.

2.3 Synchrotron radiation-based microtomography

The historical specimen was also examined at the I12 beamline of the Diamond Light Source (Didcot, Oxfordshire, United Kingdom) [20]. The sample was placed in the 3D-printed holder, see Figure 3, and to maximize stability within the holder for high-resolution scans, the sample and holder were tightly wrapped with Parafilm. The holder was then secured to the sample stage with double-sided tape.

Table 2. Acquisition parameters for the advanced laboratory-based micro computed tomography of the human gracilis muscle sample in ethanol with the Exciscope Polaris.

Parameter	Setting
Geometrical magnification	1.955
Optical magnification	20
Acceleration voltage [kV]	40
Beam current [µA]	75
Filter	none
Effective pixel size [µm]	0.3499
Number of projections	5001
Exposure time per projection [s]	22

Local tomograms were acquired using a monochromatic beam with a photon energy of 54 keV and a scintillator-based X-ray detector with a 2560 × 2160 pixel CMOS sensor. For the overview scans, the 0.346× and 0.82× magnification camera modules were used, resulting in isotropic pixel sizes of 18.53 and 7.91 µm, respectively. The local scan of the hamular region was acquired at 2.0× magnification and a resulting pixel size of 3.24 µm. Projections were acquired over 180° in 0.1° steps with an exposure time per projection of 25 ms for the overview scans, *i.e.* a total scan time of 45 s, and 100 ms for the high-resolution scan with a total scan time of 180 s.

2.4 Image reconstruction

For the laboratory-based µCT, the data were reconstructed using the manufacturer's solutions: phoenix datos|x (nanotom® m), XMReconstructor (Xradia 610 Versa), and the cloud-based proprietary reconstruction software (Exciscope Polaris). The synchrotron data were lens distortion corrected [21], flatfield- and darkfield-corrected, and phase retrieval [22] was carried out by Paganin filtering with $\delta/\beta = 250$, a value chosen on the basis of visual inspection of the reconstructed data, as it provided a sensible increase in contrast without excessive loss in spatial resolution. Images were reconstructed with the standard reconstruction pipeline savu [23] with filtered back-projection [24]. The results were exported in TIFF and HDF5 format, respectively, for the qualitative and quantitative evaluation.

2.5 Registration and segmentation

The six datasets of the specimen were rigidly registered in VGStudio MAX 2.1 (Volume Graphics, Heidelberg, Germany) by finding corresponding volumes in the laboratory- and synchrotron radiation-based datasets and manually aligning them. The quality of the registration was evaluated by visually assessing the accuracy of the alignment.

Segmentation was carried out in VGStudio MAX 2.1. Automated threshold-based segmentation was applied for rendering of the preserved bones, with specific threshold sets based on image contrast and tissue density. Automated segmentation of soft tissue structures was infeasible; hence muscle segments and aponeurosis were manually segmented in a slice-by-slice manner based on visually discernible features. Interpolation enabled smoothening of segmentation edges for the visualization purposes. For the gracilis muscle, datasets were also imported into VGStudio MAX 2.1. Tapered muscle fibers were manually identified in the high-resolution scan by visual inspection and subsequently segmented.

3. RESULTS

3.1 Comparison of microtomography setups

The high-resolution laboratory-based microtomography data of the infant head acquired with the Xradia 610 Versa system resembles the one of the synchrotron radiation-based imaging facilities in terms of spatial resolution and contrast, as indicated by the visualization of relevant microanatomical features using representative slices at the selected pixel sizes of 3.4 and 3.24 µm, respectively. Conventional full-field CT with 55 µm pixels failed to visualize the pterygoid hamulus in sufficient detail. Figure 4 displays a representative slice of the hamular region of the plastinated tissue to qualitatively compare the image quality of the experimental setups used.

Figure 4. The hamular region imaged with the nanotom® m (a), the Xradia 610 Versa (b), and the phase tomography at the synchrotron radiation facility (c).

The differentiation of fiber tracts within the soft tissues was clearest in the synchrotron radiation-based dataset after phase retrieval. This measure significantly increased the contrast compared to the absorption contrast data from the Xradia 610 Versa system, see Figure 5. The visualization of nerves, vessels, or a fat pad in the hamular region was even impossible in the phase-retrieved data.

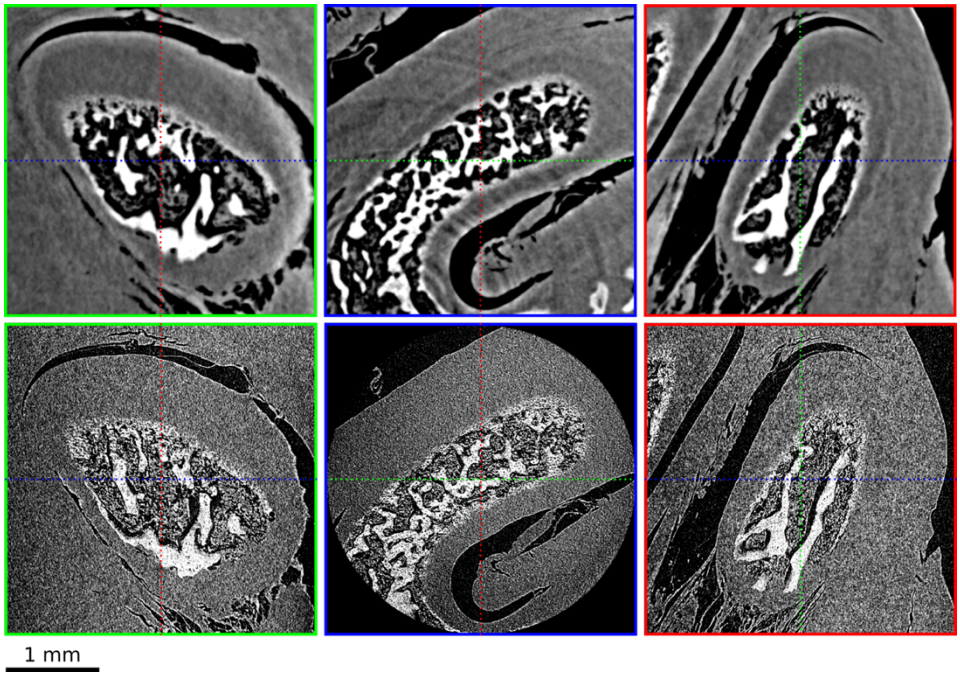

Figure 5. Three orthogonal slices through a volume of interest around the pterygoid hamulus, acquired at the beamline I12 of the Diamond Light Source (top) and using the Xradia 610 Versa µCT-system (b) (bottom).

When comparing the laboratory-based µCT images, the manual segmentation of muscle segments was especially effective using the Xradia 610 Versa data at 0.4× magnification. It was well suited to strike a balance between feature discrimination and the ability to follow fibers over a sufficiently long distance. The high level of detail provided by the 4× magnification enabled a detailed visualization of the bony microstructure.

The comparison of the histograms of the high-resolution data acquired at the synchrotron radiation facility and with the Xradia 610 Versa system with a pixel size slightly larger than 3 µm allowed us to draw conclusions on the density resolution. The monochromatic tomography data from the synchrotron radiation facility exhibit rather narrow and distinct peaks compared to the laboratory-based µCT data based on a broad energy spectrum, cf. Figure 6.

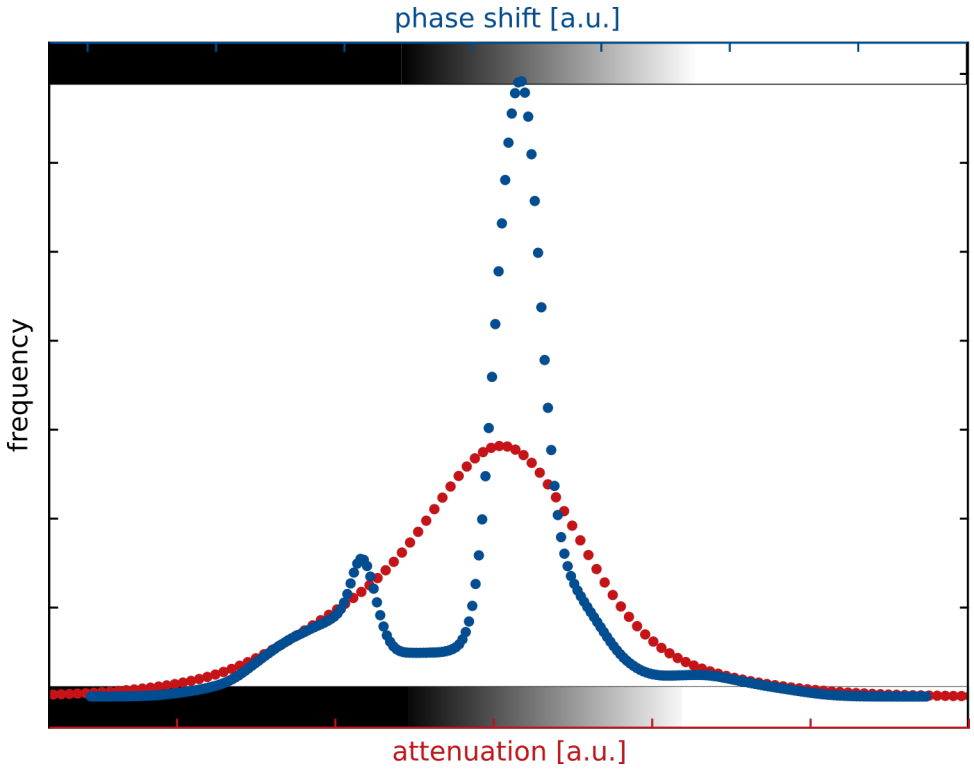

Figure 6. Histograms of tomography data with about $(3\ \mu m)^3$ voxels acquired with the Xradia 610 Versa (red dots) and with the tomography setup at the synchrotron facility (blue dots). The smeared histogram peaks observed in the conventional X-ray source data can be attributed to several factors, including image noise associated with lower beam intensity and statistics, and the broad energy spectrum.

3.2. Microanatomy around the pterygoid hamulus

The tensor veli palatini muscle was found to be composed of two distinct heads, as shown in Figure 7. The lateral head extends from the cranial base toward the pterygoid hamulus, which acts as a fulcrum and redirects the tendon medially, where it radiates into the palatine aponeurosis. The medial head originates from the Eustachian tube and ends in the inferior part of the pterygoid fossa. The superior pharyngeal constrictor muscle originates from the posterior aspect of the medial pterygoid plate and the pterygoid hamulus. The levator veli palatini muscle was identified from its origin at the cranial base and along its course parallel to the Eustachian tube to its insertion into the palatine aponeurosis. Figure 8 shows a three-dimensional rendering of the velopharyngeal muscle sling.

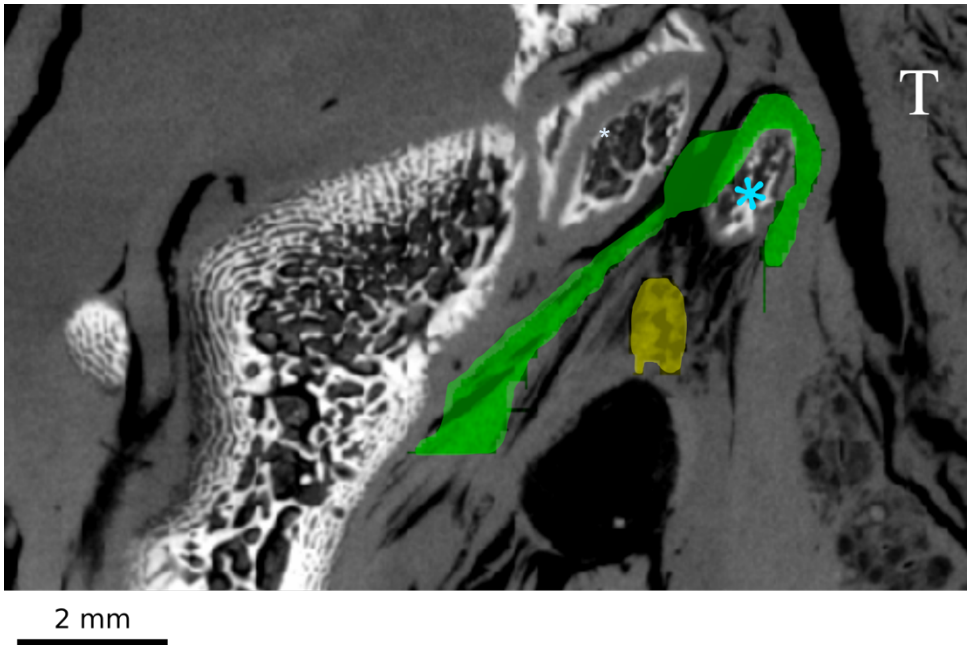

Figure 7. Laboratory-based micro computed tomography image acquired with the Xradia 610 Versa showing the lateral (green) and medial (yellow) heads of the tensor veli palatini muscle around the pterygoid hamulus (*). Note the air inclusions following the muscle fascicles, for instance in the tongue (T).

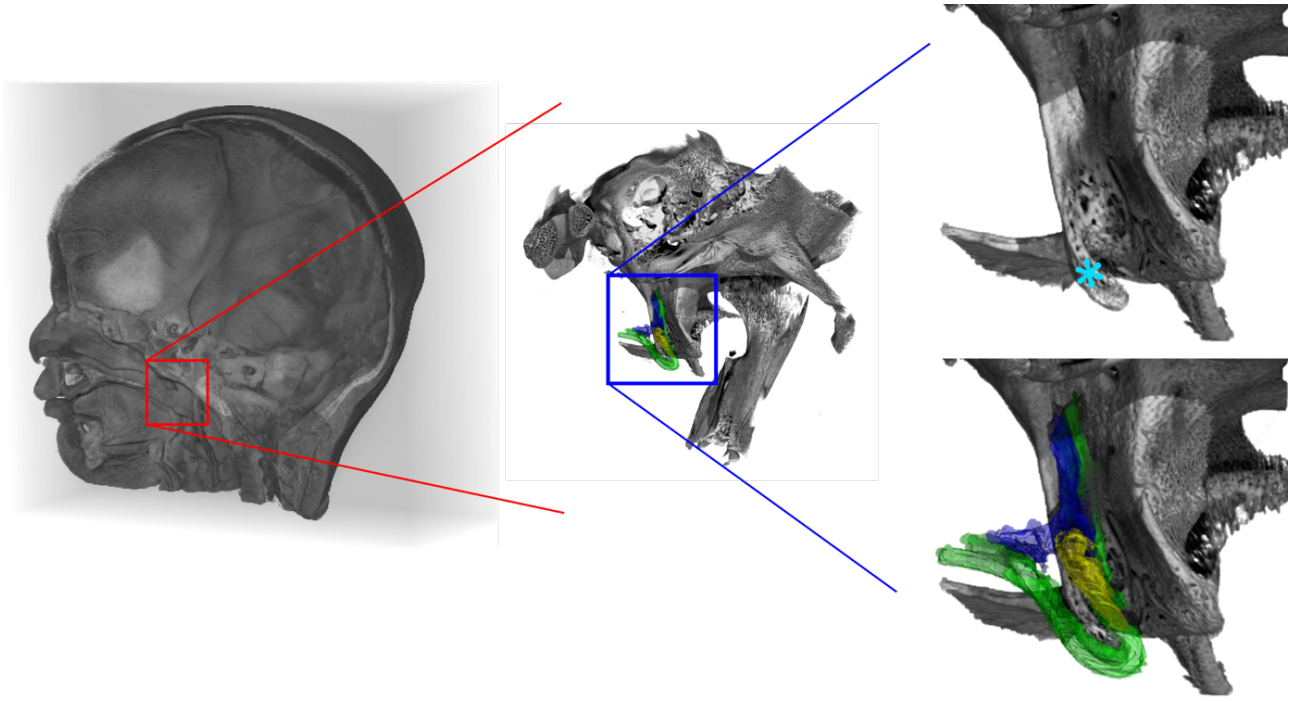

Figure 8. Three-dimensional rendering of the velopharyngeal muscle sling around the pterygoid hamulus (*) with the two distinct heads of the tensor veli palatini muscle (green: lateral head; yellow: medial head; blue: levator veli palatini muscle)

3.3 Microstructure of the pterygoid hamulus

The pterygoid hamulus was measured to obtain the overall length of 4.05 mm from its base at the sphenoid bone to its tip, with an angulation of 151° on its medial side. Distinct surface structures were observed. Some regions were smooth and covered by periosteum, while other regions were rough with exposed subperiosteal bone, as illustrated in Figure 9. The rough regions were found in closest proximity to discernible muscle fibers. They might correspond to an enthesis, where muscles attach to the bone. This hypothesis, however, could not be confirmed with the available data owing to limited soft tissue contrast.

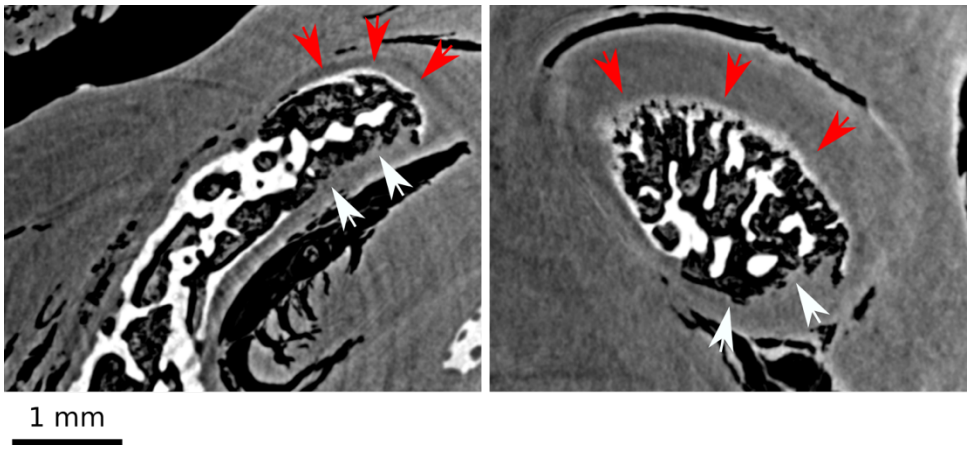

Figure 9. Hamular microtopography showing smooth (red arrows) and rough (white arrows) surface areas in coronal (left) and axial (right) slices acquired with the Xradia 610 Versa instrument.

3.4 Microanatomy of the human gracilis muscle

The gracilis muscle specimen exhibited approximately 16% shrinkage due to ethanol-based dehydration. The contrast of the muscle in PBS was insufficient to provide useful images. Superior contrast was obtained after ethanol dehydration, as illustrated by the virtual orthogonal sections in Figure 10. Individual muscle fibers were easily visible, with mitochondria visualized in the endomysium adjacent to the myofibrils and nuclei located at the periphery of the muscle fibers. The intra-fascicular termination of the tapered fibers supported the idea of an in-series arrangement of cells as suggested in a previous publication [19]. Although several fascicles were well preserved, detailed analysis was challenging in the peripheral regions, particularly in the area transitioning into the tendon, due to significant damage likely resulting from tissue handling during and after surgery, as well as the fixation and dehydration processes. Videos 1 and 2 show tapered fibers in two orthogonal planes, providing complementary views of the fiber structure.

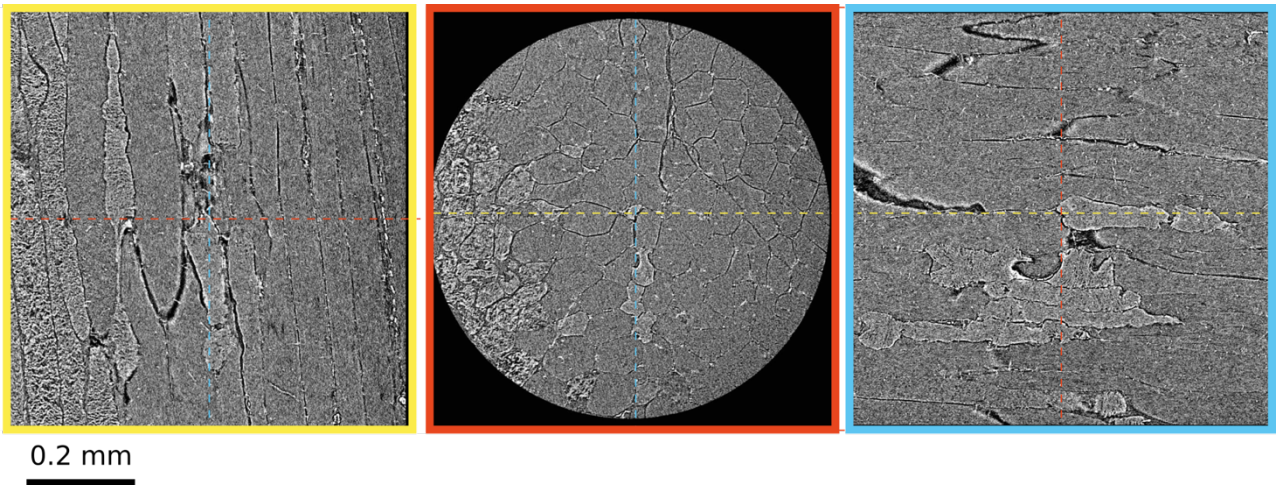

Figure 10. Three orthogonal slices through muscle fibers within the human gracilis muscle specimen suspended in 100 % ethanol. Note the tapered fibers in an in-series arrangement.

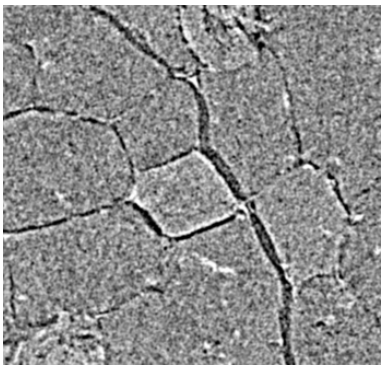

Video 1. Visualization of the micro computed tomography dataset of a human gracilis muscle sample acquired with the Exciscope Polaris. Cross-sectional view sliced perpendicular to the fiber orientation. http://dx.doi.org/10.1117/12.3035601.1

Video 2. Visualization of the micro computed tomography dataset of a human gracilis muscle sample acquired with the Exciscope Polaris. Longitudinal view sliced parallel to the fiber orientation. http://dx.doi.org/10.1117/12.3035601.2

4. DISCUSSION

4.1 Imaging

Both laboratory- and synchrotron radiation-based μCT provided high-resolution three-dimensional datasets of the hard tissues in the region of interest around the pterygoid hamulus of a historical infant cadaveric head. In the plastinated specimen, where the soft tissues were infused with a polymer, contrast within the muscles was limited, especially compared to iodine-stained tissues reported in the literature [13, 14]. Nevertheless, the boundaries between the fiber tracts within the soft tissues were discernible. This observation was most pronounced in the phase-contrast tomographic imaging. Segmentation and three-dimensional rendering of selected anatomical structures provided results that were considered adequate based on visual assessment and comparison with existing anatomical data. The directionality which was particularly pronounced in the phase-contrast tomography data, facilitated the identification of muscle fibers. Some artifacts were recognized: edge enhancement, ring and streak artifacts. These artifacts, however, did not significantly interfere with the segmentation of anatomical features.

Absorption-based tomography provided insufficient contrast between materials that had similar density and atomic composition. State-of-the-art clinical CT was limited in its ability to resolve microanatomical details. For instance, the pterygoid hamulus could hardly be visualized. The spatial resolution of μCT provided an accurate depiction of these structures, comparable to histology images after physical sectioning, but with the added advantages of being largely non-destructive and maintaining the three-dimensional orientation. This was particularly advantageous in this study for tracking the fibers as they pivoted around the pterygoid hamulus in three-dimensional space.

It is critical that valuable and unique historical specimens are not damaged during imaging studies. No visible signs of radiation damage such as bubble formation, discoloration, or thermal motion artifacts were observed in the synchrotron radiation-based scans, indicating that X-ray imaging with high photon flux is a reliable option for the non-destructive evaluation of plastinated specimens. However, damage at a molecular level, particularly alterations in DNA structure, is likely to occur in μCT imaging due to the primary beam, but also by secondary calcium and electron emissions from bone in the specimen. This must be considered if further molecular analysis is planned. It is important to note that μCT can only be used for imaging of post-mortem human tissues mainly because of the high radiation dose. Although μCT offers exceptional spatial and density resolution, its utility currently is confined to research settings rather than clinical facilities.

Synchrotron radiation-based μCT showed advantages over laboratory-based μCT, particularly in terms of density resolution, soft tissue contrast, and scan time. At three minutes, the scan time at the synchrotron facility was significantly shorter than the 40 hours with the Xradia 610 Versa. This difference in scan time becomes even more important when higher resolution is required over a large region of interest. The high photon flux of a synchrotron radiation facility in combination with a monochromator allows imaging at a well-defined, tunable photon energy.

With dedicated systems and magnification objectives, the three-dimensional imaging of ethanol-immersed soft tissue with true sub-micrometer resolution can be achieved with laboratory-based μCT, as demonstrated by the visualization of the myofibrils within the muscle cells in the human gracilis muscle sample. The imaging of an entire human gracilis muscle with laboratory-based μCT is challenging and needs a huge amount of time for data acquisition. Synchrotron radiation-based μCT offers advantages for sub-cellular resolution imaging over larger regions.

4.2. Specimens

Modern plastination techniques typically involve fixation, dehydration, and defatting of the specimen, followed by impregnation with a polymer material under vacuum conditions [25]. Earlier methods for whole-specimen preservation included formalin fixation and paraffin embedding [26]. The dehydration process is known to result in significant soft tissue shrinkage [27, 28]. The 16 % shrinkage of the gracilis muscle specimen after ethanol dehydration in this study is consistent with these previously published results. It was assumed that the air inclusions observed within the muscle tissue along the muscle fascicles in the infant head specimen were related to such shrinkage artifacts. No air inclusions other than those directly related to true anatomical features were observed, indicating a high-quality plastination process. The lack of knowledge about the specific plastination technique used on this specimen complicates interpretation and selection of

parameters for imaging and analysis. Without detailed documentation, it is impossible to base these decisions on the properties of the materials used, such as X-ray attenuation, without additional substantial and time-consuming efforts such as pre-measurements and analysis [29]. The human gracilis muscle segment showed significant damage in its periphery, likely resulting from tissue handling, fixation and dehydration processes.

The age of the infant at the time of its death is unknown. Based on its features, it is believed to have passed away in the neonatal period. Palatoplasty is usually performed at around eight to nine months of age, so the specimen examined in this study is younger than a typical surgical patient undergoing cleft palate repair [2]. The gross anatomy, especially the origin and insertion of the palatal muscles, is not expected to change significantly after birth. However, the elongation of the head along the longitudinal axis during postnatal development results in an increase in the angle between the Eustachian tube and the palate, thus altering the slope of the tensor and levator veli palatini muscles [30], and possibly affecting other features such as the composition of the peri-hamular fibrous connective tissues [31]. With a length of 4 mm, the pterygoid hamulus was shorter than in studies on adults [32, 33]. With differential growth in the maxillofacial region, the three-dimensional relationship between structures may also change, potentially altering the biomechanics of the muscle sling, such as the direction of force vectors. In addition, anatomical changes due to disease or syndromes cannot be ruled out in this historical specimen. This again highlights the importance of careful documentation of specimen characteristics to facilitate accurate interpretation of data.

Muscle segmentation was performed by a maxillofacial surgery resident (DS) familiar with the muscular structures around the pterygoid hamulus under the supervision of an expert anatomist (SM) and an experienced cleft surgeon (AAM) to ensure accurate identification of true anatomical features. Based on existing anatomical knowledge from atlases, the discernible features within the µCT images were used for segmentation. To verify that these structures directly correspond to anatomical features, correlation with a sectioned specimen, e.g., a sliced specimen embedded in methyl-methacrylate, is required [34]. Destructive dissection of this unique historical specimen was impossible for obvious reasons, and to the authors' knowledge, a similar benchmark specimen is not yet available. Therefore, some uncertainty remains regarding the assignment of features visible in the µCT dataset to the actual anatomical features.

4.3. Muscle micro-architecture

The observation of tapered and overlapping fibers in the muscle specimen marks a significant advance in the understanding of muscle microarchitecture and challenges the traditional view that muscle fibers in long muscles extend uninterrupted from their origin to the tendinous insertion. Microscopy studies have suggested a serial arrangement of muscle fibers in long muscles several decades ago, and the visualization of tapered fibers in µCT images adds a new dimension to this concept [35, 36]. The biomechanical implications, particularly in the context of surgical procedures such as muscle transplants, are substantial [19, 37]. Tapered fibers confined to only a portion of the total muscle length could influence force generation and contraction dynamics, potentially affecting the performance and functional outcomes of muscle transplants [38, 39]. However, the present study only examined a segment of the muscle, which necessitates consideration of local differences and variability within the muscle. This includes the variations in fiber type composition, which could be assessed by staining and histology. It remains unclear how common tapered fibers are across muscles or whether they are more prevalent in, or exclusive to, longer muscles such as the femoral adductors. Further research is needed to elucidate the distribution and functional significance of tapered fibers in different muscle types and to understand their implications for muscle function and surgical techniques.

4.4 Surgical conclusions for palatoplasty

The results of this study suggest a close topographic relationship between several muscles and the pterygoid hamulus. Deriving dynamic implications from findings in static imaging is difficult. It can nevertheless be hypothesized that the three-dimensional arrangement of these muscles is crucial for velopharyngeal function. Notably, the two heads of the tensor veli palatini muscle appear to have distinct and separate functions: (1) the lateral head, which extends from the cranial base via the pterygoid hamulus to the aponeurosis, likely assists in soft palate reinforcement during swallowing and articulation; and (2) the medial head, which originates from the Eustachian tube and inserts into the palatine fossa,

likely assists in opening the Eustachian tube during swallowing. Figure 11 shows a medical illustration of the two distinct parts of the muscle.

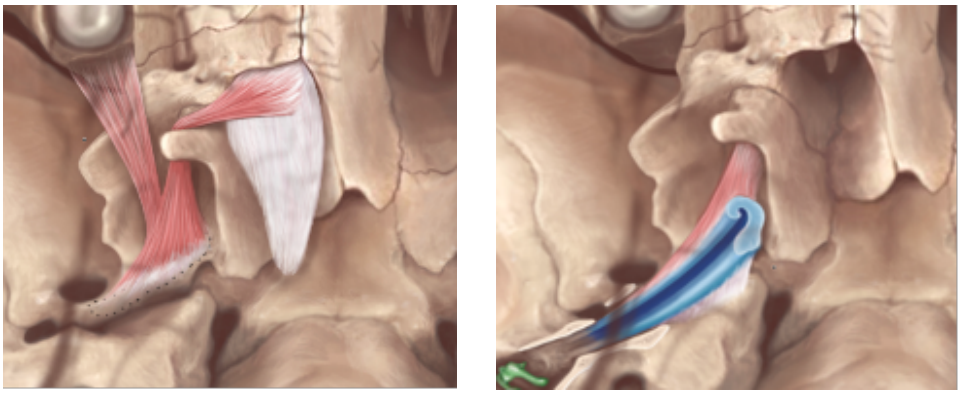

Figure 11. Medical illustrations of the two parts of the tensor veli palatini muscle with their distinct origins and insertions: Lateral head (left) and medial head (right). Illustrations by Mueller and Voll.

Surgical access from the medial side to the connection between the palatine aponeurosis and the tendon of the lateral head of the tensor veli palatini muscle may preserve the functional integrity of the Eustachian tube and the medial head of the tensor veli palatini muscle intact. In contrast, lateral approaches to the hamular region or fracturing of the pterygoid hamulus may carry a higher risk of disrupting this functional unit. The technique used in the authors' department (AAM) involves releasing the lateral tensor veli palatini tendon anteromedially to the hamulus, thus preserving the connection between the medial part of the tendon and the Eustachian tube [2]. A medial approach further respects the attachment of the superior pharyngeal constrictor muscle to the pterygoid hamulus and might thereby further support the velopharyngeal function. Combined radiographic and histological examination of a cleft specimen, ideally at the age at which cleft repair is typically performed, could help to justify surgical approaches by verifying the anatomic situation in patients with cleft palate.

5. CONCLUSIONS

Laboratory-based μCT systems proved suitable for the visualization of the palatal anatomy and the micro-architecture of unstained human skeletal muscle tissue. Synchrotron radiation-based microtomography showed added soft-tissue contrast after phase retrieval, allowing manual segmentation of muscle segments even in a plastinated specimen with limited soft-tissue contrast. The intimate anatomical and functional relationship between the velopharyngeal muscle sling and the pterygoid hamulus was confirmed. The study's findings are in line with the concept that the tensor veli palatini muscle consists of two functional parts, as opposed to the common description of a single functional part with two heads. The results of this study suggest that minimal incision palatoplasty with preservation of the hamular region may be advantageous in the surgical treatment of cleft palate to preserve velopharyngeal and Eustachian tube function.

ACKNOWLEDGEMENTS

The authors express their gratitude to Andreas Roser (Core Facility 3D Print Lab, Department of Biomedical Engineering, University of Basel) for his expertise in the design and fabrication of the specimen holder, and to Dr. Griffin Rodgers for proofreading the manuscript. This work was carried out with the support of Diamond Light Source (proposal MG36969).

REFERENCES

[1] P. Naidu, C. A. Yao, D. K. Chong *et al.*, "Cleft Palate Repair: A History of Techniques and Variations," Plast Reconstr Surg Glob Open, 10(3), e4019 (2022).

[2] B. K. Benitez, A. Brudnicki, Z. Surowiec *et al.*, "Continuous circular closure in unilateral cleft lip and plate repair in one surgery," J Craniomaxillofac Surg, 50(1), 76-85 (2022).

[3] B. Schonmeyr, and P. Sadhu, "A review of the tensor veli palatine function and its relevance to palatoplasty," J Plast Surg Hand Surg, 48(1), 5-9 (2014).

[4] M. Abe, G. Murakami, M. Noguchi *et al.*, "Variations in the tensor veli palatini muscle with special reference to its origin and insertion," Cleft Palate Craniofac J, 41(5), 474-84 (2004).

[5] K. Sumida, Y. Ando, S. Seki *et al.*, "Anatomical status of the human palatopharyngeal sphincter and its functional implications," Surg Radiol Anat, 39(11), 1191-1201 (2017).

[6] K. H. Koch, M. A. Grzonka, and J. Koch, "Pathology of the palatal aponeurosis in cleft palate," Cleft Palate Craniofac J, 35(6), 530-4 (1998).

[7] K. H. Koch, M. A. Grzonka, and J. Koch, "The pathology of the velopharyngeal musculature in cleft palates," Ann Anat, 181(1), 123-6 (1999).

[8] S. R. Rood, and W. J. Doyle, "Morphology of tensor veli palatini, tensor tympani, and dilatator tubae muscles," Ann Otol Rhinol Laryngol, 87(2 Pt 1), 202-10 (1978).

[9] M. W. Halle, R. Kikinis, and P. E. Neumann, "TA2Viewer: A web-based browser for Terminologia Anatomica and online anatomical knowledge," Clin Anat, 37(6), 640-648 (2024).

[10] M. Kitajiri, I. Sando, and T. Takahara, "Postnatal development of the eustachian tube and its surrounding structures. Preliminary study," Ann Otol Rhinol Laryngol, 96(2 Pt 1), 191-8 (1987).

[11] A. Khimchenko, H. Deyhle, G. Schulz *et al.*, "Extending two-dimensional histology into the third dimension through conventional micro computed tomography," Neuroimage, 139, 26-36 (2016).

[12] M. N. Holme, G. Schulz, H. Deyhle *et al.*, "Complementary X-ray tomography techniques for histology-validated 3D imaging of soft and hard tissues using plaque-containing blood vessels as examples," Nat Protoc, 9(6), 1401-15 (2014).

[13] W. Di, J. Zhao, H. Ma *et al.*, "Three-Dimensional Anatomy of the Palatopharyngeus and Its Relation to the Levator Veli Palatini Based on Micro-Computed Tomography," Plast Reconstr Surg, 148(3), 389e-397e (2021).

[14] J. Zhao, H. Ma, Y. Wang *et al.*, "Micro-Computed Tomography-Based Three-Dimensional Anatomical Structure of the Region Around the Pterygoid Hamulus," Cleft Palate Craniofac J, 59(7), 918-925 (2022).

[15] J. Zhao, H. Ma, Y. Wang *et al.*, "Cadaveric Study and Micro-Computed Tomography of the Anatomy of Palatine Aponeurosis and its Link to the Soft Palate Muscles and Pharyngeal Muscles," Cleft Palate Craniofac J, 60(3), 319-326 (2023).

[16] N. S. Jeffery, R. S. Stephenson, J. A. Gallagher *et al.*, "Micro-computed tomography with iodine staining resolves the arrangement of muscle fibres," J Biomech, 44(1), 189-92 (2011).

[17] S. H. Jang, J. Lee, and O. Lee, "Micro- and nano-tomography analysis of mouse soleus muscle using radiation," Microsc Res Tech, 84(11), 2685-2693 (2021).

[18] M. Walters, M. Crew, and G. Fyfe, "Bone Surface Micro-Topography at Craniofacial Entheses: Insights on Osteogenic Adaptation at Muscle Insertions," Anat Rec (Hoboken), 302(12), 2140-2155 (2019).

[19] B. I. Binder-Markey, L. S. Persad, A. Y. Shin *et al.*, "Direct intraoperative measurement of isometric contractile properties in living human muscle," J Physiol, 601(10), 1817-1830 (2023).

[20] M. Drakopoulos, T. Connolley, C. Reinhard *et al.*, "I12: the Joint Engineering, Environment and Processing (JEEP) beamline at Diamond Light Source," J Synchrotron Radiat, 22(3), 828-38 (2015).

[21] N. T. Vo, R. C. Atwood, and M. Drakopoulos, "Radial lens distortion correction with sub-pixel accuracy for X-ray micro-tomography," Optics Express, 23(25), 32859-32868 (2015).

[22] D. Paganin, S. C. Mayo, T. E. Gureyev *et al.*, “Simultaneous phase and amplitude extraction from a single defocused image of a homogeneous object,” Journal of Microscopy, 206(1), 33-40 (2002).

[23] R. C. Atwood, A. J. Bodey, S. W. T. Price *et al.*, “A high-throughput system for high-quality tomographic reconstruction of large datasets at Diamond Light Source,” Philosophical Transactions of the Royal Society A: Mathematical, Physical and Engineering Sciences, 373(2043), 20140398 (2015).

[24] W. van Aarle, W. J. Palenstijn, J. Cant *et al.*, “Fast and flexible X-ray tomography using the ASTRA toolbox,” Optics Express, 24(22), 25129-25147 (2016).

[25] B. M. Riederer, “Plastination and its importance in teaching anatomy. Critical points for long-term preservation of human tissue,” J Anat, 224(3), 309-15 (2014).

[26] C. von Horst, R. von Hagens, C. M. Sora *et al.*, “History and development of plastination techniques,” Anat Histol Embryol, 48(6), 512-517 (2019).

[27] U. A. Shetty, C. Dinakar, A. M. D'Cruz *et al.*, “Plastination - A method for preservation of oral hard and soft tissue biopsy specimen v/s the conventional method of preservation with formalin,” J Oral Maxillofac Pathol, 27(3), 515-519 (2023).

[28] G. Rodgers, W. Kuo, G. Schulz *et al.*, “Virtual histology of an entire mouse brain from formalin fixation to paraffin embedding. Part 1: Data acquisition, anatomical feature segmentation, tracking global volume and density changes,” J Neurosci Methods, 364, 109354 (2021).

[29] P. Shanthi, R. R. Singh, S. Gibikote *et al.*, “Comparison of CT numbers of organs before and after plastination using standard S-10 technique,” Clin Anat, 28(4), 431-5 (2015).

[30] P. P. Le Floch-Prigent, J. Nguyen, and J. B. Gillot, “Valsalva: “de aure humane tractatus…” 1707, Utrecht: The second edition of the seminal treatise on the structure of the ear,” The FASEB Journal, 33(S1), (2019).

[31] Y. Orita, I. Sando, M. Miura *et al.*, “Postnatal changes in the connective tissue in the region lateral to the eustachian tube: possible relationship to tube function,” Ann Otol Rhinol Laryngol, 112(8), 716-21 (2003).

[32] N. Malkidou, K. Chaidas, V. Thomaidis *et al.*, “Pterygoid Hamulus: Morphological Analysis and Clinical Implications,” Cureus, 16(3), e55694 (2024).

[33] A. Mehra, F. R. Karjodkar, K. Sansare *et al.*, “Assessment of the dimensions of the pterygoid hamulus for establishing age- and sex-specific reference standards using cone-beam computed tomography,” Imaging Sci Dent, 51(1), 49-54 (2021).

[34] S. E. Mezey, M. Muller-Gerbl, M. Toranelli *et al.*, “The human masseter muscle revisited: First description of its coronoid part,” Ann Anat, 240, 151879 (2022).

[35] M. I. Heron, and F. J. Richmond, “In-series fiber architecture in long human muscles,” J Morphol, 216(1), 35-45 (1993).

[36] M. Young, A. Paul, J. Rodda *et al.*, “Examination of intrafascicular muscle fiber terminations: implications for tension delivery in series-fibered muscles,” J Morphol, 245(2), 130-45 (2000).

[37] R. J. Monti, R. R. Roy, J. A. Hodgson *et al.*, “Transmission of forces within mammalian skeletal muscles,” J Biomech, 32(4), 371-80 (1999).

[38] P. P. Purslow, and J. A. Trotter, “The morphology and mechanical properties of endomysium in series-fibred muscles: variations with muscle length,” J Muscle Res Cell Motil, 15(3), 299-308 (1994).

[39] J. Douglas, S. Pearson, A. Ross *et al.*, “Chronic Adaptations to Eccentric Training: A Systematic Review,” Sports Med, 47(5), 917-941 (2017).